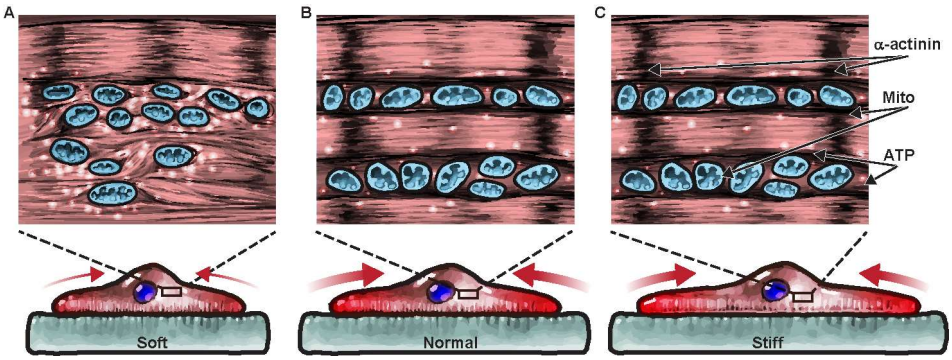

Fig 4. Cardiomyocytes operate optimally on substrates of physiological stiffness possibly due to a link between metabolism and contractile structure and function. Based on our data, we speculated that substrate stiffness might regulate the balance of energy production and utilization in cardiac tissues as follows. Cardiomyocytes on soft gels (A) need abundant ATP (white spheres) derived by mitochondria (orange organelles) to promote the contraction of sarcomeres (Z-disks in black) via cross-bridge cycling (brown lines). This might lead to very inefficient mechanical work as only a small stress (red arrows) is required to deform the soft gel substantially. Conversely, NRVM cultured on normal (B) and stiff (C) substrates have well organized contractile cytoskeletons and need a limited amount of ATP to fuel sarcomere contraction. Since the same amount of contractile force causes a smaller displacement of stiffer gels, the product between force and displacement (work) is maximum on gels of physiological stiffness.

https://doi.org/10.1371/journal.pone.0194706.g004

consistent with our experience with TFM in single cells and cell pairs, stamping of gels with stiffness less than five kPa remains difficult. Therefore, a better stamping technique might be needed to obtain the larger sample sizes needed to tease apart smaller contractile differences in cells seeded on substrates with stiffness values in the fetal range (e.g., 1, 3, and 5 kPa).

As a proof-of-concept study, we combined our mTissue TFM platform with an industry-standard high-throughput metabolic flux analyzers to investigate the coupling between mechanotransduction, contractility, and metabolism. We speculate (Fig 4) that myocytes on soft substrate might require a larger amount of ATPs than cells on stiffer substrates, as they must complete the assembly of the contractile cytoskeleton in addition to performing their contractile activity. We showed that NRVM on gels with normal physiological stiffness reached an optimum coupling between energy production and energy consumption; that is, cells on substrates mimicking physiological stiffness needed the minimum amount of ATP to generate the maximum amount of work. On stiffer substrates, ATP levels and the cell-generated stress did not change leading to an overall reduction in displacement and work. Conversely, on softer substrates, NRVM had the largest amount of ATP available to generate the minimum amount of work via an immature contractile apparatus [4, 19]. An efficiency metric can be used to characterize the coupling between energy production (metabolism) and energy utilization (sarcomerogenesis and contractility) in cardiomyocytes; that is, the ratio between the contractile work done by the cells and the metabolic energy provided by the mitochondria [38]. To compare contractile work and oxygen consumption rates, we converted [pMol/min] of ATP into the corresponding [pJ/beat] values using the following assumptions. First, NRVM beat 120 times in a minute under the 2Hz pacing. Second, the surface area of a Seahorse well is 550x larger than a diamond tissue surface area, leading to a similar increase in cell number [16]. And third, a Mole of ATP provides ~29 kJ of energy [39]. With these approximations, our results demonstrate that tissues engineered on substrates of physiological stiffness convert metabolic energy into contractile work ~2x and ~200x better than they do on stiffer and softer substrates, respectively. One limitation of this analysis is that we only partially control for the cell beating frequency. In fact, intrinsic beating activity in primary [40–42] and stem cell-derived cardiomyocytes [43, 44] changed as much as 20% and 300% as a function of substrate

stiffness and the type of preparation. Here, we minimized the difference between spontaneous metabolism and stimulated contractility by choosing the smallest pacing frequency (2 Hz) that overdrove the NRVM intrinsic activity. To overcome this limitation in future efforts, we envision using optical pacing of cells expressing light-sensitive ion channels [45].

In conclusion, the tissue-level assay presented here completes a consistent suite of TFM-based assays that can enable thorough multi-scale studies of the coupling between metabolism, mechanotransduction, and contractility in primary and stem cell-derived myocytes [5–8]. Two recent studies from Prof. McCain's group addressed similar topics: tissue-level cardiac TFM [46] and NRMV metabolism as a function of substrate stiffness [47]. While these studies are consistent with our findings, a few important differences exist. For example, they engineered NRVM in square-shaped tissues on normal and stiff gels using fibronectin and laminin cues [46] we used larger, diamond-shaped Fibronectin-only cues to improve cellular alignment in mTissues cultured on soft, normal, and stiff gels. Consistent with our study, stiffening of the substrate caused a sharp decline in cell-induced deformation and contractile work in engineered tissues, independently from the chosen ECM ligand. Similarly, to obtain substrates of pathological stiffness, we had to cast hydrogels directly into the very small wells of the Seahorse plate and could only culture randomly-oriented NRVM (1, 13, and 90 kPa). Instead, the metabolic difference between randomly-oriented and laminar tissues was studied [47] by engineering cells on transferrable elastomeric substrates prepared in a range of stiffness that greatly exceeds the pathophysiological range (1, 27, and 2700 kPa). In contrast to our findings, a reduced metabolic activity was observed on NRVM cultured on soft substrates under both laminar and non-laminar conditions. We attribute this difference to the distinct chemical and viscoelastic properties of elastomers and hydrogels that may influence the density of printed ECM proteins and cellular behavior [48, 49]. We believe engineered cardiac tissues will become progressively more important as in studying the energetic coupling underpinning cardiac development and homeostasis [12, 15], and might inform the design of better differentiation and maturation protocols for hiPS-derived cardiomyocytes [4, 19].

Materials and methods

Cardiac myocyte harvest, seeding, and culture

All animal procedures conducted in this study were approved by the Harvard University Animal Care and Use Committee. Cardiac myocytes were extracted from neonatal rat ventricles using a previously described method [7, 8]. Left ventricle tissue was isolated from neonate (p2) Sprague-Dawley rats (Charles River) that were sacrificed after ethanol-based anesthetization. Cells were isolated using overnight trypsinization at 4˚ C and serial collagenase digestions at room temperature. A highly pure cardiomyocyte population was obtained by differential adhesion using two pre-plating steps. Cardiomyocytes were cultured on engineered substrates in 6-well plates at a density of 100,000 cells/cm^2 in Medium 199 supplemented with 10% heat-inactivated fetal bovine serum (FBS, Invitrogen, Carlsbad, CA), 10 mM HEPES, 0.1 mM MEM non-essential amino acids, 20 mM glucose, 2 mM L-glutamine, 1.5 μM vitamin B-12, and 50 U/mL penicillin for 1 day. The serum concentration was reduced to 2% after 24 hr to minimize proliferation of the small pool of fibroblast present in the culture. Cells were cultured for four days before conducting the experiments.

Gel fabrication and microcontact printing

Polyacrylamide gel substrates were fabricated and characterized as previously described in details [7, 8]. Specifically, three groups of gels were created by varying the acrylamide/bis composition. Soft gels were obtained mixing 5/0.1% acrylamide/bis components and had a Young

modulus of 0.9±0.02 kPa (nominal stiffness 1 kPa). Normal gels were obtained mixing 7.5/0.3% acrylamide/bis and had a Young modulus of 13±0.1 kPa (nominal stiffness 13 kPa). Stiff gels were obtained mixing 12/0.6% acrylamide/bis and had a Young modulus of 90±1.5 kPa (nominal stiffness 90 kPa). Furthermore, streptavidin-acrylamide and fluorescent beads (200 n m) were added to a final concentration (by volume) of 1:5 and 1:100, respectively to permit binding biotinylated-fibronectin (Sulfo-NHS-LC-Biotin, Pierce). Gels polymerized while sandwiched between glutaraldehyde-activated and inactivated coverslips before drying the gel surface (37 ˚C for 10 minutes) and microcontact printing with biotinylated FN.

Photo- and soft-lithography were conducted as previously described in details [7, 8, 10]. Specifically, a photolithographic mask carrying the desired diamond and frame features was designed in AutoCAD (Autodesk Inc.) and manufactured at the Center for Nanoscale Systems at Harvard University. Silicon molds to fabricate polydimethylsiloxane (PDMS, Sylgard 184, Dow Corning) stamps were prepared by spin-coating SU-8 2002 photoresist (MicroChem Corp) on silicon wafers (Wafer World) that were exposed to UV light through the photoligraphic mask in a mask aligner (ABM Inc.)and then developed in propylene-glycol-methyl-ether-acetate to dissolve the masked regions. The resulting PDMS stamps were coated with 200 μg/mL biotinylated FN and incubated for 1 hr before stamping on pre-dried streptavidin-doped polyacrylamide gels.

Contractility assay and electrical field stimulation

Traction force microscopy experiments were conducted as previously described [7, 8, 10]. On day 4 of culture, cardiac mTissues in modified Tyrode's solution (1.8 mM $CaCl_2$, 5 mM glucose, 5 mM HEPES, 1 mM $MgCl_2$, 5.4 mM KCl, 135 mM NaCl, 0.33 mM NaH_2PO_4, pH 7.4) were imaged on an environmental controlled line scanning confocal microscope (Zeiss LSM510) using a 40X air objective (with a 0.5x zoom) or a 20x objective to ensure the full diamond-shaped tissue fit within the diagonal of the field of view. Movies of contracting myocytes and bead displacement were imaged at 33 Hz with both brightfield, and 488 laser excitation and recordings were performed over multiple [6–10] contractile cycles. Differently, than single-cell or cell-pair assays, mTissues could be electrically paced to control the beating rate using two custom-made platinum electrodes inserted onto the lid of a 35mm petri dish and connected to an external field stimulator (Myopacer, IonOptix Corp., Milton, MA). Recordings were conducted at 2 Hz and using voltages between 8 to 11 V that reliably overdrove spontaneous beating in the mTissues.

Contractility analysis

The methods used to acquire displacement and traction stress vectors from images of bead displacement have been previously described [7, 18]. Briefly, a displacement field was determined by comparing bead images throughout the contraction cycle to the bead image at diastole. The traction stress field was then calculated from the displacement map using constrained Fourier transform traction cytometry. Importantly, we used the bright field video acquired together with the bead displacement to define the boundary of the mTissue in calculating the traction field. Moreover, the contractile traction force field was calculated from the displacement field using the Boussinesq solution and assuming the substrate as an elastic half-space with known mechanical properties (stiffness of 1, 13, or 90 kPa and Poisson ratio assumed to be 0.5). Notably, this particular assumption, important in accelerating the calculations needed to obtain a traction field, becomes less accurate as the size of the contractile elements grow larger than the thickness of the tissue [50–52]. We used a more accurate boundary element method [18] that admits a Green function characteristic of gels with finite thickness [53] to estimate the error

and found that peak systolic stress and contractile work are slightly overestimated (1–15%) with the simple FTTC method. At the same time the more accurate analysis took ~10 hr/frame on a powerful workstation computer to vs ~3 min/frame in the case of the simpler FTTC analysis. Since we processed 300 frames worth of gel deformation per mTissues, we utilized the faster, if slightly less accurate, analysis in this study.

Immunostaining and structure determination

Image analysis and processing were performed as previously described [5]. After the contractility assay, samples were incubated for 15 minutes in 4% Paraformaldehyde (PFA) and 0.5μl/ml of TritonX-100 in PBS at 37˚C before washing in PBS and incubation with 200 μl primary antibody solution containing 1 DAPI, 1 μl Alexa Fluor633-conjugated Phalloidin (Invitrogen, Carlsbad, CA), 1 μl polyclonal anti-human fibronectin antibody (F2648, Sigma-Aldrich, St. Louis, MO), and 1 μl monoclonal anti-sarcomeric α-actinin for 1 hour at room temperature. Samples were then washed three times in PBS and incubated for 1 hour with a goat anti-rabbit Alexa Fluor-546 antibody and a goat anti-mouse Alexa Fluor-488 antibody (Invitrogen, 1:200 dilution). The samples were washed three times again in PBS and mounted on microscope glass slides in prolongGold (Invitrogen) that cured for at least 48 hr before fluorescent imaging on a Zeiss LSM 510 confocal microscope. Sarcomere length and sarcomere packing density were determined using a Fourier-based method previously described [19].

Seahorse metabolic measurements

Cellular metabolism was measured using a Seahorse Bioscience XFe 24 Extracellular Flux Analyzer (North Billerica, MA). Polyacrylamide gels were pipetted into the wells (10 mL/well) of a standard XF24 microplate (Seahorse Bioscience, North Billerica, MA) and allowed to crosslink before rinsing with PBS. Plates were stored at 4 ˚C until cell seeding with neonatal rat ventricular myocytes (100 000 cells/100 mL/well). After seeding, plates were left in the laminar flow hood for 30 min to minimize edge effects before transfer to a 37 ˚C, 5% CO_2 incubator. After two hours, 500 mL of media was added to each well and media exchanges were performed as previously described above. After four days in culture, culture media was replaced with XF Assay Medium (Seahorse Bioscience, North Billerica, MA) supplemented with 20 mM glucose and plates were incubated at a 37 C for 1 h. The proprietary hydrated cartridge was loaded with 2 mM oligomycin, 1 mM carbonyl cyanide-4-(trifluoromethoxy) phenylhydrazone (FCCP), and 1 mM antimycin A and 1 mM rotenone from the XF Cell Mito Stress Test Kit (Seahorse Bioscience, North Billerica, MA). The cartridge and cell plate were then inserted into the Seahorse XFe 24 Extracellular Flux Analyzer (North Billerica, MA), which made three measurements of baseline oxygen consumption rate (OCR) and three OCR measurement after injection of each of the drugs listed above. Data from multiple wells across three different neonatal rat ventricular myocyte harvest cycles were collected and used for analysis.

Statistical analysis

Through the text, our results are presented as mean ± standard error of the mean (s.e.m.). After verifying that the data points were normally distributed (Shapiro-Wilkinson test), statistical comparisons were conducted among the various group using 1-way ANOVA test followed by Tukey pairwise comparisons. All analyses were conducted using SigmaPlot (Systat Software, Inc.–CA, USA). The symbol * was used to denote statistically significant difference characterized by a p-value smaller than 0.05.

Supporting information

S1 Checklist. The ARRIVE guidelines checklist.
(PDF)

Acknowledgments

The authors are grateful to Prof. Megan McCain for valuable discussions and would like to thank Michael Rosnach for the figure illustrations. The authors also acknowledge support from NIH NCATS UH2 and UH3 awards TR000522 "Human Cardiopulmonary System-On-a-Chip," DARPA BAA-11-73 "Human Microphysiological Systems Program," and NSF Materials Research Science and Engineering Center (MRSEC) grant DMR-1420570. Parts of this work were performed at the Harvard University Center for Nanoscale Systems (CNS), a member of the National Nanotechnology Infrastructure Network (NNIN), which is supported by NSF award ECS-0335765. The funders had no role in study design, data collection, and analysis, decision to publish, or preparation of the manuscript.

Author Contributions

Conceptualization: Francesco Silvio Pasqualini, Ashutosh Agarwal, Kevin Kit Parker.

Data curation: Francesco Silvio Pasqualini, Ashutosh Agarwal.

Formal analysis: Francesco Silvio Pasqualini, Ashutosh Agarwal, Qihan Liu.

Funding acquisition: Kevin Kit Parker.

Investigation: Francesco Silvio Pasqualini, Ashutosh Agarwal, Blakely Bussie O'Connor, Sean P. Sheehy, Kevin Kit Parker.

Methodology: Francesco Silvio Pasqualini, Ashutosh Agarwal, Blakely Bussie O'Connor, Qihan Liu.

Project administration: Francesco Silvio Pasqualini, Kevin Kit Parker.

Resources: Francesco Silvio Pasqualini, Ashutosh Agarwal, Sean P. Sheehy.

Software: Francesco Silvio Pasqualini.

Supervision: Francesco Silvio Pasqualini, Ashutosh Agarwal, Kevin Kit Parker.

Validation: Ashutosh Agarwal, Kevin Kit Parker.

Visualization: Francesco Silvio Pasqualini, Ashutosh Agarwal.

Writing – original draft: Francesco Silvio Pasqualini, Ashutosh Agarwal, Kevin Kit Parker.

Writing – review & editing: Francesco Silvio Pasqualini, Ashutosh Agarwal, Blakely Bussie O'Connor, Qihan Liu, Sean P. Sheehy, Kevin Kit Parker.

References

1. Chabiniok R, Wang VY, Hadjicharalambous M, Asner L, Lee J, Sermesant M, et al. Multiphysics and multiscale modelling, data-model fusion and integration of organ physiology in the clinic: ventricular cardiac mechanics. Interface focus. 2016; 6(2):20150083. https://doi.org/10.1098/rsfs.2015.0083 PMID: 27051509
2. Parker KK, Ingber DE. Extracellular matrix, mechanotransduction and structural hierarchies in heart tissue engineering. Philosophical transactions of the Royal Society of London Series B, Biological sciences. 2007; 362(1484):1267–79. https://doi.org/10.1098/rstb.2007.2114 PMID: 17588874

3. Sheehy SP, Grosberg A, Qin P, Behm DJ, Ferrier JP, Eagleson MA, et al. Toward improved myocardial maturity in an organ-on-chip platform with immature cardiac myocytes. Experimental biology and medicine (Maywood, NJ). 2017:1535370217701006.
4. Sheehy SP, Pasqualini F, Grosberg A, Park SJ, Aratyn-Schaus Y, Parker KK. Quality metrics for stem cell-derived cardiac myocytes. Stem cell reports. 2014; 2(3):282–94. https://doi.org/10.1016/j.stemcr.2014.01.015 PMID: 24672752
5. Aratyn-Schaus Y, Pasqualini FS, Yuan H, McCain ML, Ye GJ, Sheehy SP, et al. Coupling primary and stem cell-derived cardiomyocytes in an in vitro model of cardiac cell therapy. The Journal of cell biology. 2016; 212(4):389–97. https://doi.org/10.1083/jcb.201508026 PMID: 26858266
6. Ribeiro AJ, Denisin AK, Wilson RE, Pruitt BL. For whom the cells pull: Hydrogel and micropost devices for measuring traction forces. Methods (San Diego, Calif). 2016; 94:51–64.
7. McCain ML, Yuan H, Pasqualini FS, Campbell PH, Parker KK. Matrix elasticity regulates the optimal cardiac myocyte shape for contractility. American journal of physiology Heart and circulatory physiology. 2014; 306(11):H1525–39. https://doi.org/10.1152/ajpheart.00799.2013 PMID: 24682394
8. McCain ML, Lee H, Aratyn-Schaus Y, Kleber AG, Parker KK. Cooperative coupling of cell-matrix and cell-cell adhesions in cardiac muscle. Proceedings of the National Academy of Sciences of the United States of America. 2012; 109(25):9881–6. https://doi.org/10.1073/pnas.1203007109 PMID: 22675119
9. Schoen I, Hu W, Klotzsch E, Vogel V. Probing cellular traction forces by micropillar arrays: contribution of substrate warping to pillar deflection. Nano letters. 2010; 10(5):1823–30. https://doi.org/10.1021/nl100533c PMID: 20387859
10. Agarwal A, Goss JA, Cho A, McCain ML, Parker KK. Microfluidic heart on a chip for higher throughput pharmacological studies. Lab on a chip. 2013; 13(18):3599–608. https://doi.org/10.1039/c3lc50350j PMID: 23807141
11. Lind JU, Busbee TA, Valentine AD, Pasqualini FS, Yuan H, Yadid M, et al. Instrumented cardiac microphysiological devices via multimaterial three-dimensional printing. Nature materials. 2017; 16(3):303–8. https://doi.org/10.1038/nmat4782 PMID: 27775708
12. McCain ML, Sheehy SP, Grosberg A, Goss JA, Parker KK. Recapitulating maladaptive, multiscale remodeling of failing myocardium on a chip. Proceedings of the National Academy of Sciences of the United States of America. 2013; 110(24):9770–5. https://doi.org/10.1073/pnas.1304913110 PMID: 23716679
13. Wang G, McCain ML, Yang L, He A, Pasqualini FS, Agarwal A, et al. Modeling the mitochondrial cardiomyopathy of Barth syndrome with induced pluripotent stem cell and heart-on-chip technologies. Nature medicine. 2014; 20(6):616–23. https://doi.org/10.1038/nm.3545 PMID: 24813252
14. Hinson JT, Chopra A, Nafissi N, Polacheck WJ, Benson CC, Swist S, et al. HEART DISEASE. Titin mutations in iPS cells define sarcomere insufficiency as a cause of dilated cardiomyopathy. Science (New York, NY). 2015; 349(6251):982–6.
15. Pasqualini FS, Nesmith AP, Horton RE, Sheehy SP, Parker KK. Mechanotransduction and Metabolism in Cardiomyocyte Microdomains. BioMed research international. 2016; 2016:4081638. https://doi.org/10.1155/2016/4081638 PMID: 28044126
16. McCain ML, Agarwal A, Nesmith HW, Nesmith AP, Parker KK. Micromolded gelatin hydrogels for extended culture of engineered cardiac tissues. Biomaterials. 2014; 35(21):5462–71. https://doi.org/10.1016/j.biomaterials.2014.03.052 PMID: 24731714
17. Grosberg A, Alford PW, McCain ML, Parker KK. Ensembles of engineered cardiac tissues for physiological and pharmacological study: heart on a chip. Lab on a chip. 2011; 11(24):4165–73. https://doi.org/10.1039/c1lc20557a PMID: 22072288
18. Han SJ, Oak Y, Groisman A, Danuser G. Traction microscopy to identify force modulation in subresolution adhesions. Nature methods. 2015; 12(7):653–6. https://doi.org/10.1038/nmeth.3430 PMID: 26030446
19. Pasqualini FS, Sheehy SP, Agarwal A, Aratyn-Schaus Y, Parker KK. Structural phenotyping of stem cell-derived cardiomyocytes. Stem cell reports. 2015; 4(3):340–7. https://doi.org/10.1016/j.stemcr.2015.01.020 PMID: 25733020
20. Dabiri GA, Turnacioglu KK, Sanger JM, Sanger JW. Myofibrillogenesis visualized in living embryonic cardiomyocytes. Proceedings of the National Academy of Sciences of the United States of America. 1997; 94(17):9493–8. PMID: 9256510
21. Villari B, Campbell SE, Hess OM, Mall G, Vassalli G, Weber KT, et al. Influence of collagen network on left ventricular systolic and diastolic function in aortic valve disease. Journal of the American College of Cardiology. 1993; 22(5):1477–84. PMID: 8227808
22. van Heerebeek L, Hamdani N, Handoko ML, Falcao-Pires I, Musters RJ, Kupreishvili K, et al. Diastolic stiffness of the failing diabetic heart: importance of fibrosis, advanced glycation end products, and

myocyte resting tension. Circulation. 2008; 117(1):43–51. https://doi.org/10.1161/CIRCULATIONAHA.107.728550 PMID: 18071071

23. Zile MR, Baicu CF, Gaasch WH. Diastolic heart failure—abnormalities in active relaxation and passive stiffness of the left ventricle. The New England journal of medicine. 2004; 350(19):1953–9. https://doi.org/10.1056/NEJMoa032566 PMID: 15128895

24. Annoni G, Luvara G, Arosio B, Gagliano N, Fiordaliso F, Santambrogio D, et al. Age-dependent expression of fibrosis-related genes and collagen deposition in the rat myocardium. Mechanisms of ageing and development. 1998; 101(1–2):57–72. PMID: 9593313

25. Dranka BP, Benavides GA, Diers AR, Giordano S, Zelickson BR, Reily C, et al. Assessing bioenergetic function in response to oxidative stress by metabolic profiling. Free radical biology & medicine. 2011; 51(9):1621–35.

26. Baillargeon B, Rebelo N, Fox DD, Taylor RL, Kuhl E. The Living Heart Project: A robust and integrative simulator for human heart function. European journal of mechanics A, Solids. 2014; 48:38–47. https://doi.org/10.1016/j.euromechsol.2014.04.001 PMID: 25267880

27. Genet M, Lee LC, Baillargeon B, Guccione JM, Kuhl E. Modeling Pathologies of Diastolic and Systolic Heart Failure. Annals of biomedical engineering. 2016; 44(1):112–27. https://doi.org/10.1007/s10439-015-1351-2 PMID: 26043672

28. Lee LC, Genet M, Acevedo-Bolton G, Ordovas K, Guccione JM, Kuhl E. A computational model that predicts reverse growth in response to mechanical unloading. Biomechanics and modeling in mechanobiology. 2015; 14(2):217–29. https://doi.org/10.1007/s10237-014-0598-0 PMID: 24888270

29. Grosberg A, Gharib M. A dynamic double helical band as a model for cardiac pumping. Bioinspiration & biomimetics. 2009; 4(2):026003.

30. Grosberg A, Gharib M. Computational models of heart pumping efficiencies based on contraction waves in spiral elastic bands. Journal of theoretical biology. 2009; 257(3):359–70. https://doi.org/10.1016/j.jtbi.2008.11.022 PMID: 19109980

31. Grosberg A, Gharib M. Modeling the macro-structure of the heart: healthy and diseased. Medical & biological engineering & computing. 2009; 47(3):301–11.

32. Broeckel U. What Can hiPSC-Cardiomyocytes Teach Us about Modeling Complex Human Disease Phenotypes? Cell stem cell. 2016; 19(3):282–4. https://doi.org/10.1016/j.stem.2016.08.016 PMID: 27588742

33. Tiburcy M, Hudson JE, Balfanz P, Schlick SF, Meyer T, Chang Liao ML, et al. Defined Engineered Human Myocardium with Advanced Maturation for Applications in Heart Failure Modelling and Repair. Circulation. 2017.

34. Abaci HE, Shuler ML. Human-on-a-chip design strategies and principles for physiologically based pharmacokinetics/pharmacodynamics modeling. Integrative biology: quantitative biosciences from nano to macro. 2015; 7(4):383–91.

35. Maass C, Stokes CL, Griffith LG, Cirit M. Multi-functional scaling methodology for translational pharmacokinetic and pharmacodynamic applications using integrated microphysiological systems (MPS). Integrative biology: quantitative biosciences from nano to macro. 2017.

36. Stokes CL, Cirit M, Lauffenburger DA. Physiome-on-a-Chip: The Challenge of "Scaling" in Design, Operation, and Translation of Microphysiological Systems. CPT: pharmacometrics & systems pharmacology. 2015; 4(10):559–62.

37. Wikswo JP, Curtis EL, Eagleton ZE, Evans BC, Kole A, Hofmeister LH, et al. Scaling and systems biology for integrating multiple organs-on-a-chip. Lab on a chip. 2013; 13(18):3496–511. https://doi.org/10.1039/c3lc50243k PMID: 23828456

38. Smith NP, Barclay CJ, Loiselle DS. The efficiency of muscle contraction. Progress in biophysics and molecular biology. 2005; 88(1):1–58. https://doi.org/10.1016/j.pbiomolbio.2003.11.014 PMID: 15561300

39. Curtis H, Barnes NS. Biology: W. H. Freeman; Fifth Edition edition (April 15, 1989); 1989.

40. Engler AJ, Carag-Krieger C, Johnson CP, Raab M, Tang HY, Speicher DW, et al. Embryonic cardiomyocytes beat best on a matrix with heart-like elasticity: scar-like rigidity inhibits beating. Journal of cell science. 2008; 121(Pt 22):3794–802. https://doi.org/10.1242/jcs.029678 PMID: 18957515

41. Shapira-Schweitzer K, Seliktar D. Matrix stiffness affects spontaneous contraction of cardiomyocytes cultured within a PEGylated fibrinogen biomaterial. Acta biomaterialia. 2007; 3(1):33–41. https://doi.org/10.1016/j.actbio.2006.09.003 PMID: 17098488

42. Jacot JG, Kita-Matsuo H, Wei KA, Chen HS, Omens JH, Mercola M, et al. Cardiac myocyte force development during differentiation and maturation. Annals of the New York Academy of Sciences. 2010; 1188:121–7. https://doi.org/10.1111/j.1749-6632.2009.05091.x PMID: 20201894

43. Ribeiro AJ, Ang YS, Fu JD, Rivas RN, Mohamed TM, Higgs GC, et al. Contractility of single cardiomyocytes differentiated from pluripotent stem cells depends on physiological shape and substrate stiffness. Proceedings of the National Academy of Sciences of the United States of America. 2015; 112 (41):12705–10. https://doi.org/10.1073/pnas.1508073112 PMID: 26417073

44. Hazeltine LB, Simmons CS, Salick MR, Lian X, Badur MG, Han W, et al. Effects of substrate mechanics on contractility of cardiomyocytes generated from human pluripotent stem cells. International journal of cell biology. 2012; 2012:508294. https://doi.org/10.1155/2012/508294 PMID: 22649451

45. Park SJ, Gazzola M, Park KS, Park S, Di Santo V, Blevins EL, et al. Phototactic guidance of a tissue-engineered soft-robotic ray. Science (New York, NY). 2016; 353(6295):158–62.

46. Ariyasinghe NR, Reck CH, Viscio AA, Petersen AP, Lyra-Leite DM, Cho N, et al. Engineering micromyocardium to delineate cellular and extracellular regulation of myocardial tissue contractility. Integrative biology: quantitative biosciences from nano to macro. 2017; 9(9):730–41.

47. Lyra-Leite DM, Andres AM, Petersen AP, Ariyasinghe NR, Cho N, Lee JA, et al. Mitochondrial function in engineered cardiac tissues is regulated by extracellular matrix elasticity and tissue alignment. American journal of physiology Heart and circulatory physiology. 2017; 313(4):H757–h67. https://doi.org/10.1152/ajpheart.00290.2017 PMID: 28733449

48. Nam S, Hu KH, Butte MJ, Chaudhuri O. Strain-enhanced stress relaxation impacts nonlinear elasticity in collagen gels. Proceedings of the National Academy of Sciences of the United States of America. 2016; 113(20):5492–7. https://doi.org/10.1073/pnas.1523906113 PMID: 27140623

49. Chaudhuri O. Viscoelastic hydrogels for 3D cell culture. Biomaterials Science. 2017; 5(8):1480–90. https://doi.org/10.1039/c7bm00261k PMID: 28584885

50. Tang X, Tofangchi A, Anand SV, Saif TA. A Novel Cell Traction Force Microscopy to Study Multi-Cellular System. PLOS Computational Biology. 2014; 10(6):e1003631. https://doi.org/10.1371/journal.pcbi.1003631 PMID: 24901766

51. Mertz AF, Banerjee S, Che Y, German GK, Xu Y, Hyland C, et al. Scaling of Traction Forces with the Size of Cohesive Cell Colonies. Physical Review Letters. 2012; 108(19):198101. https://doi.org/10.1103/PhysRevLett.108.198101 PMID: 23003091

52. Banerjee S, Marchetti MC. Contractile Stresses in Cohesive Cell Layers on Finite-Thickness Substrates. Physical Review Letters. 2012; 109(10):108101. https://doi.org/10.1103/PhysRevLett.109.108101 PMID: 23005331

53. Merkel R, Kirchgessner N, Cesa CM, Hoffmann B. Cell force microscopy on elastic layers of finite thickness. Biophysical journal. 2007; 93(9):3314–23. https://doi.org/10.1529/biophysj.107.111328 PMID: 17660320